

Statistical Analysis of Yttrium-Doped ZnO Nanoparticles for Gas Sensing Applications

Satender Kumar¹, Ankur Nehra^{2*}

¹Department of Physics (School of Science) Sunrise University, Alwar, Rajasthan, India

²Department of Mathematics, Dhanauri P.G. College, Dhanauri, Haridwar, Uttarakhand, India

ABSTRACT

Yttrium-doped ZnO (YZ) thin films were synthesized using sol-gel spin coating technique on planar glass substrates. Their optical and electrical properties were analyzed to assess their potential for O₂ gas detection. XRD analysis confirmed a hexagonal wurtzite crystal structure, while FE-SEM images revealed a network of spherical nanoparticles. Optical transmission spectra showed that increasing Y-dopant concentration widened the bandgap from 3.27 eV to 3.30 eV. Electrical measurements indicated that YZ3 exhibited highest conductivity. Gas sensing performance was evaluated for YZ2 and YZ4 at an O₂ flow rate of 450 sccm and an operating temperature of 70°C. Among them, YZ4 demonstrated the highest response, reaching a value of 1, with a fast response time of 2 seconds and a recovery time of 4 seconds. Statistical analysis suggests that YZ thin films hold promise for efficient gas sensing at lower operating temperatures.

Keywords: YZ thin films, Electrical properties, Gas sensing, Sol-gel, Synthetic material

1. Introduction

The capability of non-toxic gases like O₂, H₂, and Ar to detect gases, generate chemicals, monitor air quality, and fuel gas-powered engines has garnered scientific interest for its applications in clinical diagnostics [1, 2]. Oxygen gas is an odorless, combustible gas that is essential to many organisms' ability to survive. Examples of semiconductor metal oxides that are necessary for gas distinction are ZnO, TiO₂, and CdO. ZnO has been considered the ideal material for gas detection applications because of its superior substance dependability, warmth under operating settings, and remarkable adaptability to lead electrons [3-8]. Due to its large band hole (3.37 eV) and high excitation energy (60 meV), ZnO is a very promising material for a variety of uses, including gas sensors, photodetectors, Schottky diodes, and photocatalysis [9]. Modern warming heaters and underground mine O₂ gas screening use ZnO-based oxygen sensors. Numerous factors, including deformities, particle size, surface characteristics, blockage level and width, and stoichiometry, influence the properties of sensors [10-11]. Doping ZnO with metals, non-metals, and interesting earth metals can reduce its resistivity [12]. These rare earth metals stand out from one another because they are predecessors of ZnO dopants, which suppress the local point defect concentrations of ZnO. La, Sc, and Y are examples of uncommon earth minerals that are widely used in a variety of applications due to their strong conductivity, consistent electrochemical responses, and iridescent qualities [13-19]. Yttrium (Y) doping in ZnO has a significant effect on the identification of O₂ gas, as demonstrated by the changed optical and electrical characteristics of ZnO and the more noticeable ionic radii of Y³⁺ (1.01 Å) compared to Zn²⁺ (0.66 Å) [20-23]. Meanwhile, ZnO has been doped with Y to improve its optical band hole and conductivity, making it more appropriate for gas detection applications [24-25]. The size and surface form of ZnO was entirely altered by the proper concentration of Y doping. Additionally, doping ZnO has been demonstrated by Guo et al. [26] to alter its surface charge regions, which impacts the material's use, particularly

for gas detection applications. Despite the data, ZnO tiny videos' union of kink-type morphology is excellent and more accurate for detecting O₂ gas. The dynamic surface region that the sensor uses to perform responses at the sensor surface represents the sensor reaction. A suitable dynamic surface region will therefore most likely successfully ascend the sensor reaction for the gas finding [27]. For slim film preparedness, a variety of witness tactics have been put forth, including the sol-gel approach [29-30], beat laser, splash pyrolysis [28], and synthetic fume statement. The sol-gel process is the most advantageous of them all since it is low cost, offers large region coatings, has an excellent material structure, and provides basic creation [31]. In this work, pure and Y-doped ZnO thin films were produced on a glass substrate via the sol-gel procedure. The main optical and morphological features of the thin films were described. Furthermore, oxygen gas's gas-detecting properties have also been taken into consideration.

2. Experimental Details

Yttrium acetic acid derivation di-hydrate (C₆H₁₄O₇Y; immaculateness 099.9%), 2-methoxy ethanol (C₃H₈O₂; immaculateness 099.0%), monoethanolamine (C₂H₇NO; virtue 099.9%), and zinc acetic acid derivation di-hydrate (C₄H₁₀O₆Zn; virtue 098.0%) were the materials and synthetic compounds used in the trial. Alfa Aesar supplied all the materials and synthetics used in the analysis, requiring no further sanitization. Prior to the claim, the substrates had been properly treated with (CH₃)₂CO, ultrasonically sonicated at a steady voltage, and cleaned by the cleaner. Every synthetic material and reagent was utilized exactly as it was obtained. After mixing ZnO with Y (Y=0, 0.50, 01.0, and 1.5 at. %) in 2-methoxy ethanol for 20 minutes, the material was ready. Subsequently, one drop at a time, stabilizer specialist mono ethanolamine was applied to each arrangement, and the mixture was stirred for a further two hours at room temperature. Thus, uniform simple configurations were obtained, and as a result, all replies for maturing 24 hours were obtained to outline all substantive

*Corresponding author: nehradpgc123@gmail.com

responses among them. Furthermore, turn-covering units employed the obtained arrangements for the statement of small-scale films. Throughout the affidavit of every example, the testimony rate was maintained at 2500.00 rpm/30 s, and the samples were then dried at 200° C. To achieve the perfect thickness of the slight films, the cycles were repeated several times. Finally, the thin films were heated to 450° C for one hour in a silent heater to promote genuine crystallinity and remove impurities. Codes YZ1, YZ2, YZ3, and YZ4 were given to ZnO doped with Y that included 0.0, 0.50, 01.0, and 1.50 at. % of Y Slim films, which were mixed at the same time. X-ray diffraction (XRD) (Philips X'pert Favorable to diffractometer) was used to analyze the primary features of small films from YZ1 to YZ4. YZ meager videos were transported using a UV-Vis spectrophotometer (Shimadzu 3600.00), and their surface morphology was examined using an electron microscope (SEM) (Zeiss Super 60.00). Two test electrometers (Keithly-4200.00 SCS) were used to assess the I-V characteristics, and a gas detection system was used to look at the gas reaction of films that were comparable to our past research [32].

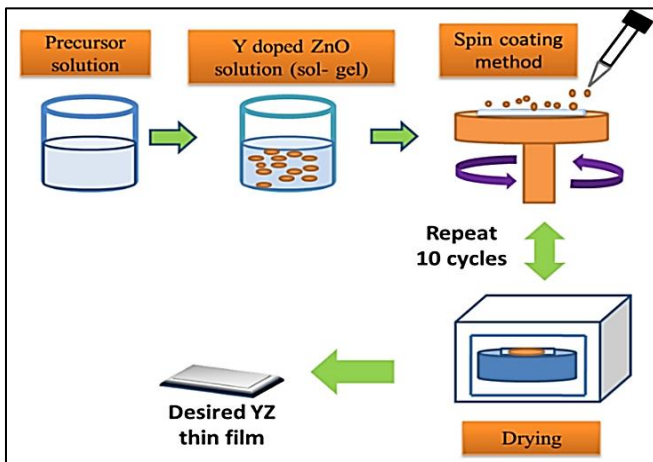


Fig. 1: Schematic Diagram for the Production of YZO Thin Film

3. Main Results with Discussion

The XRD analysis of the YZO thin film test results is shown in Figure 2. In the diffraction example of YZO tests, many tops were found at planes (001), (002), (101), (102), and (110). Based on XRD analysis, all of the YZO thin films are polycrystalline and match the wurtzite hexagonal structure of JCPDS card number 36-1451 (ZnO). It was shown that when the doping degree of Y grows, the ZnO tops become more distributed and varied in power compared to undoped ZnO (YZ1). By widening the yttrium focus, the diversity in force is linked to the enhancement of gem formation. Furthermore, the XRD design did not include any pollutants or extra pinnacles, indicating that Y particles replace ZnO locations or interstitial destinations [33, 34]. Moreover, there was neither left nor right shifting, which produced excellent agreement with the typical ZnO results. Using Eq. 1, the grid limits 'a' and 'c' were evaluated at (100) and (002) tops, respectively, and discussed in Table 1.

$$\frac{1}{d^2} = \frac{4}{3a^2} (h^2 + hk + k^2) + \frac{l^2}{c^2} \quad (1)$$

Furthermore, no contaminants or extra pinnacles were added to the XRD design, indicating that Y particles replace ZnO locations or interstitial destinations [33, 34]. Moreover, neither left nor right moving was present, which greatly agreed with the typical ZnO results. Table 1 presents the results of the evaluation of the grid boundaries 'a' and 'c' at (100) and (002) tops, respectively, using Eq. 1.

$$D = 0.94\lambda/\beta \cos\theta \quad (2)$$

Where the usual bounds are denoted by θ , β , and λ [35]. As shown in Table 1, it was discovered that increasing the doping of Y in ZnO changed the value of crystallite size.

Table 1: Y-Doped ZnO meagre films: optical limit and underlying layers

Sample Code	Peak position (2θ)	Lattice parameter a (Å)	Lattice parameter c (Å)	Crystalline size (nm)	Optical band gap (Eg) (eV)
YZ1	036.121	03.241	05.23	18.00	03.27
YZ2	036.220	03.249	05.23	17.00	03.128
YZ3	036.520	03.247	05.23	10.00	03.129
YZ4	036.319	03.252	05.23	12.00	03.130

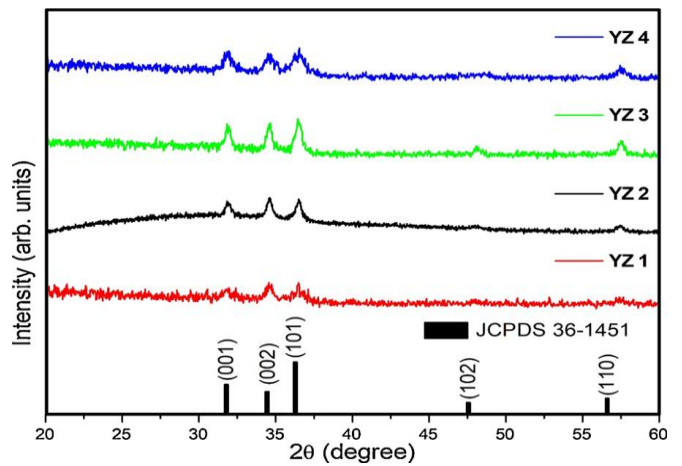


Fig. 2: XRD pattern of Y doped ZnO (Y=0.0, 0.5, 1, 1.5at%) thin film samples coded as YZ1, YZ2, YZ3 and YZ4

3.1. Surface Structure

The FESEM was used to examine the surface morphology of YZ thin films, as Figure 3 illustrates. SEM scans showed that, at low magnification, all thin films had wrinkle-type morphology, as shown in Figures 3(a), (c), (e), and (d). These fault networks were made up of tiny, spherical nanoparticles. This kind of crumpled morphology may have been molded by compressive film forces because a YZ-put-together configuration was maintained with respect to a glass substrate during the combination cycle [36–37]. The difference in warm development coefficients then surfaced in the fragile film drying system, which motivated the gelated-based slight film twisting technique. As can be shown in Figure 3 (b, d, f, and h), higher amplification usually reveals that thin films have oval and round-type morphology. In this way, the grains were arranged in a more granular form and suitably interconnected.

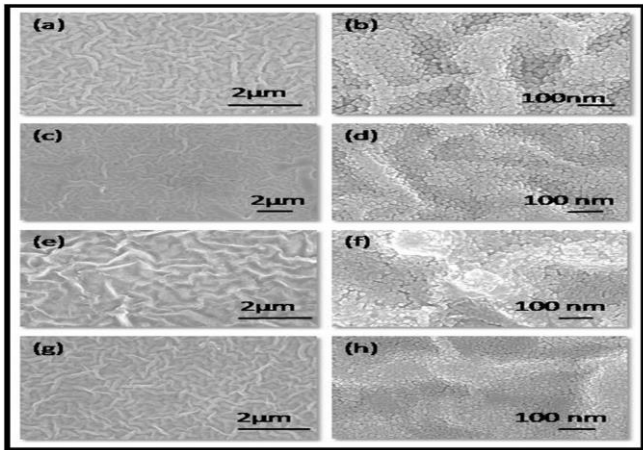


Fig. 3: FESEM pictures show ZnO doped with Y.

3.2. Optical Study

The transmission spectra of the slight films of YZ1, YZ2, YZ3, and YZ4 were kept within the 300–800 nm frequency range, as Fig. 4(a) illustrates. As Yttrium doping in ZnO increased, the typical conveyance increased in the notable region for testing from YZ1 to YZ4, as shown in Fig. 4(a). In the meantime, there was no discernible difference between the contaminated and pure samples' retention margins. The reduction of the spaces in the example is directly related to the improvement in apparent conveyance. In this way, it expands the distribution and enhances the homogeneous design. Furthermore, the standard conveyance was directly related to grain size. The grain size changed, but just a little. In the obvious location, typical conveyance therefore only changed from 92% to 97%. Consequently, a critical rise in straightforwardness was not achieved by raising the doping concentration of Y in ZnO. Rana et al. [33] have also explained similar results for Mg-doped ZnO setup using a sol-gel turn covering technique. In due course, Tauc's plot was employed to evaluate the optical bandgap of the samples using Eq. 3.

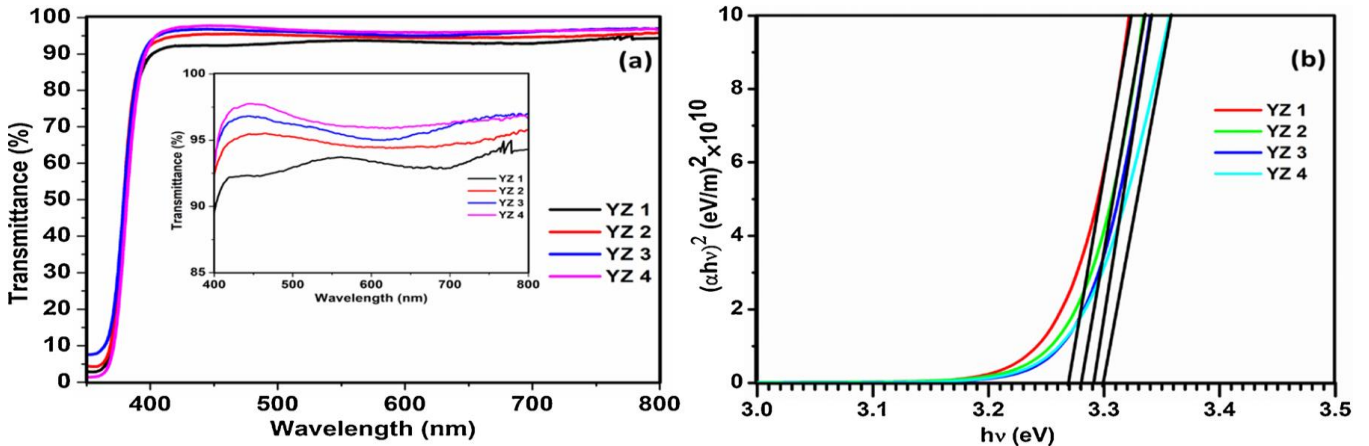


Figure 4: Optical properties of ZnO thin-film doped with Y: Transmission (a) and optical band gap (b)

$$(\alpha h\nu)^2 = A(h\nu - E_g) \quad (3)$$

where $h\nu$ is the occurrence energy, A is the proportionality consistent, E_g addresses the example's band hole, and α addresses the retention coefficient. The band gap was calculated by extrapolating the direct parcel from the $(\alpha h\nu)^2$ vs $h\nu$ plot, as explained in Fig. 4(b) [38]. Table 1 illustrates how the estimated bandgap changed as the Y doping focus increased, going from 3.27 eV to 3.30 eV. The optical band hole saw had a small alteration due to the low yttrium doping in ZnO. This could be a result of Y's fermi level, which is associated with the Greenery Burstein influence and is located inside ZnO's conduction band. Similar outcomes were shown by Thirumoorthi et al. [34] when Y-doped ZnO thin films were made by the sol-gel turn covering technique.

3.3. Electrical Characteristics

Figure 5 shows the current-voltage (I-V) characteristics of the thin films YZ1, YZ2, YZ3, and YZ4. Research has shown that while the conductivity of the thin film was lower for test YZ4, it was higher for test YZ3 when the Y doping level in ZnO was increased [39, 40]. The whole diversity in the conductivity of YZO dainty flicks was caused by the straightforward substitution of Y^{3+} in Zn^{2+} locations with essentially no grid twisting. Expanding the electrical conductivity is caused by introducing additional free electrons into the conduction band, as demonstrated by the YZ1 to YZ3 tests. From that point on, The SEM image in Fig. 3(h) makes clear that the conductivity was decreased for the YZ4 test, and the cause was grain limit dispersion and isolation of Y at the grain limit. That being said, the YZ4 test's electrical conductivity was more notable than the pure ZnO test (YZ1 test). Ozturk and colleagues similarly reported similar outcomes. Moreover, the film's outer layer and crystallinity also affect how the conductivity varies. Similarly, the dopants and defects have a major role in regulating the conductivity of the thin layer. Furthermore, the SEM micrograph's flaw-type morphology could give electrons a clear route to travel, increasing electrical conductivity [34] and improving sensor response.

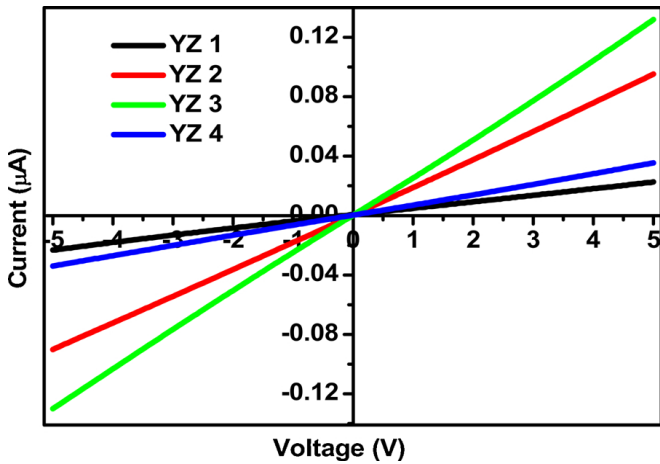
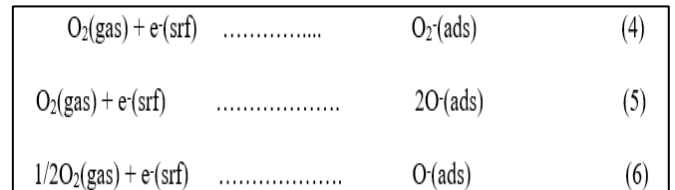


Fig. 5: I-V characteristics of thin films YZ1, YZ2, YZ3, and YZ4 are shown in this Figure

3.4 Gas Sensing

The restricted film output of YZ was optimized for gas detection. The quality of the diamonds and the electrical responsiveness of the thin sheets are two factors that affect the detecting reaction. All YZ slim films have a gem structure, which is confirmed by the XRD design. Better electrical outcomes were anticipated in every situation, as shown by the SEM pictures' kink-type surface topology. It was determined that the YZ2 test's defect type morphology was useful for identifying O₂ gas, while improvements in awareness of CO₂ gas were shown by Basyooni et al. [42] using the Na-ZnO nanostructured defect type morphology. Additionally, the I-V research shows that the YZ4 thin film's conductivity is the most noteworthy. The YZ slight film tests were judged to have exhibited oxygen detection at a convergence of 450 sccm. In our environment, oxygen is a readily available gas that interacts with the surface of metal oxides to function as an electron acceptor, ionizes, and forms a superficial ionic layer that aids in the retention of vaporous particles. One important limit for gas-detecting applications is working temperature. The stability of the sensor response is displayed in Fig. 6(a). The voltage rises quickly and stabilizes when O₂ gas enters the test chamber. When the O₂ gas is taken out of the test chamber, the voltage returns to its

starting point. For the YZ2 and YZ4 experiments, the sensor reaction/recuperation times were observed at around 2 s/3 s and 2 s/4 s, respectively. Furthermore, the YZ2 thin film's suitability for the gas reaction is demonstrated in Fig. 6(b), where the reaction bend is almost constant. For the YZ4 test, the highest sensor reaction was recorded at 70° C, with a reaction esteem of 1. Compared to YZ4, At all operating temperatures, YZ2's sensor response was poorer. Because the kink-type morphology facilitates easy electron movement and produces better electrical results, the morphology at the surface level was directly responsible for the detecting reaction.



4. Conclusion

Yttrium-doped ZnO (YZ) thin films were successfully synthesized using the sol-gel spin coating technique on flat glass substrates. Their structural, optical, and electrical properties were analyzed to assess their potential for O₂ gas detection. XRD analysis confirmed a hexagonal wurtzite crystal structure, while FE-SEM images revealed spherical nanoparticles forming a network. Optical transmission spectra showed that increasing Y-dopant concentration widened the bandgap from 3.27 eV to 3.30 eV. Electrical analysis indicated that YZ3 exhibited the highest conductivity.

Gas sensing performance was evaluated for YZ2 and YZ4 at an O₂ flow rate of 450 sccm and an operating temperature of 70°C. Among them, YZ4 demonstrated the highest gas response, reaching a value of 1, with a fast response time of 2 seconds and a recovery time of 4 seconds. These findings suggest that YZ thin films are promising candidates for gas detection applications at lower operating temperatures, as supported by statistical analysis.

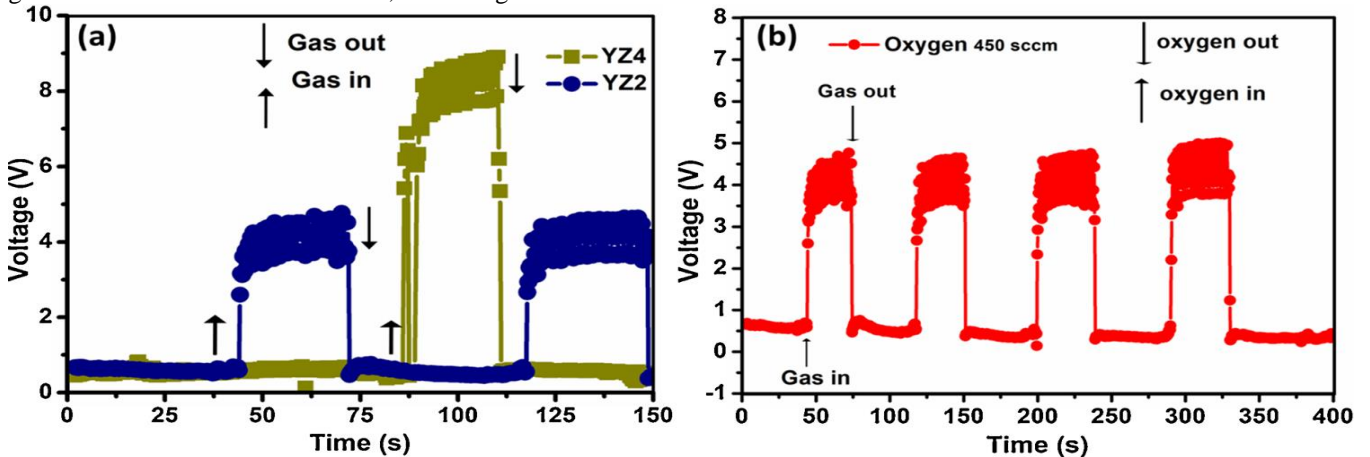


Fig. 6: Curve of Sensor Response

References

- [1] R. T. R. Kumar, J. Grabowska, J. P. Mosnier, M. O. Henry, and E. McGlynn, "Morphological control of ZnO nanostructures grown on silicon in integrated optoelectronic devices," *Proc. SPIE*, vol. 6474, pp. 64741, 2007.
- [2] C. Y. Lu, S. P. Chang, S. J. Chang, T. J. Hsueh, C. L. Hsu, Y. Z. Chiou, and I. C. Chen, "ZnO nanowire-based oxygen gas sensor," *IEEE Sens. J.*, vol. 9, no. 4, pp. 485–489, 2009.
- [3] N. Kumar, R. Kaur, and R. M. Mehra, "Characterization of sol-gel derived yttrium-doped n-ZnO/p-Si heterostructure," *Mater. Sci. Poland*, vol. 24, pp. 375–383, 2006.
- [4] V. Kumar, V. Kumar, S. Soma, L. P. Purohit, O. M. Ntwaeaborwa, and H. C. Swart, "Role of swift heavy ion irradiation on the emission of boron-doped ZnO thin films for near white light application," *J. Alloys Compd.*, vol. 594, pp. 32–38, 2014.
- [5] T. K. Pathak, V. Kumar, H. C. Swart, and L. P. Purohit, "P-type conductivity in doped and co-doped ZnO thin films synthesized by RF magnetron sputtering," *J. Mod. Opt.*, vol. 62, pp. 1368–1373, 2015.
- [6] R. C. Singh, M. P. Singh, O. Singh, P. S. Chandi, and R. Kumar, "Effect of 100 MeV O⁷⁺ ions irradiation on ethanol sensing response of nanostructures of ZnO and SnO₂," *Appl. Phys.*, vol. 98, pp. 161–166, 2010.
- [7] V. Galstyan, E. Comini, C. Baratto, G. Faglia, and G. Sberveglieri, "Nanostructured Zn chemical gas sensor," *Ceram. Int.*, vol. 41, pp. 14239–14244, 2015.
- [8] G. K. Upadhyay, J. K. Rajput, T. K. Pathak, and P. K. Pal, "Tailoring and optimization of hybrid ZnO: TiO₂: CdO nanomaterials for advanced oxidation process under visible light," *Appl. Surf. Sci.*, vol. 509, pp. 145326, 2020.
- [9] G. K. Upadhyay, J. K. Rajput, T. K. Pathak, and V. Kumar, "Synthesis of ZnO: TiO₂ nanocomposites for photocatalyst application in visible light," *Vacuum*, vol. 160, pp. 154–163, 2019.
- [10] G. Korotcenkov, "Handbook of Gas Sensor Materials: Properties, Advantages and Shortcomings for Applications," Volume 1: Conventional Approaches, Springer, New York, Heidelberg, Dordrecht, London, vol. 1, pp. 442–454, 2013.
- [11] M. J. Madou and S. R. Morrison, *Chemical Sensing with Solid State Devices*, Academic Press, London, vol. 19, pp. 342–348, 1989.
- [12] P. Singh, R. Kumar, and R. K. Singh, "Progress on transition metal-doped ZnO nanoparticles and its application," *Ind. Eng. Chem. Res.*, vol. 58, pp. 17130–17163, 2019.
- [13] L. Cheng, S. Y. Ma, X. B. Li, J. Luo, W. Q. Li, F. M. Li, Y. Z. Mao, T. T. Wang, and Y. F. Li, "Highly sensitive acetone sensors based on Y-doped SnO₂ prismatic hollow nanofibers synthesized by electrospinning," *Sens. Actuators B: Chem.*, vol. 200, pp. 181–190, 2014.
- [14] M. Hjiri, R. Dhahri, K. Omri, L. E. Mir, S. G. Leonardi, N. Donato, and G. Neri, "Effect of indium doping on ZnO-based gas sensor for CO," *Mater. Sci. Semicond. Process.*, vol. 27, pp. 319–325, 2014.
- [15] S. A. Hakim, Y. Liu, Y. Lu, and W. Chen, "Room temperature highly selective ethanol sensing behavior of hydrothermally prepared Te-V₂O₅ nanorod nanocomposites," *Mater. Sci. Semicond. Process.*, vol. 31, pp. 630–638, 2015.
- [16] R. C. Singh, O. Singh, M. P. Singh, P. S. Chandi, and R. Thangaraj, "Sensing behavior of nanosized zinc-tin composite oxide towards liquefied petroleum gas and ethanol," *Mater. Res. Bull.*, vol. 45, no. 9, pp. 1162–1164, 2010.
- [17] C. Y. Tee, G. K. Das, Y. Zhang, and T. T. Yang, "Rare earth nanophosphors in light-emitting diodes," in *Rare Earth Nanotechnology*, Singapore: Pan Stanford Publishing Pte. Ltd., pp. 203–244, 2012.
- [18] J. Steckl, J. H. Park, and J. M. Zavada, "Prospects for rare earth doped GaN lasers on Si," *Mater. Today*, vol. 10, pp. 20–27, 2007.
- [19] V. Kumar, O. M. Ntwaeaborwa, J. Holsa, D. E. Motaung, and H. C. Swart, "The role of oxygen and titanium-related defects on the emission of TiO₂:Tb³⁺ nano-phosphor for blue lighting applications," *Opt. Mater.*, vol. 46, pp. 510–516, 2015.
- [20] W. Shide, L. Chao, W. Wei, W. Huanxin, S. Yangliang, Z. Youqi, and L. Lingzhen, "Nd-doped SnO₂: characterization and its gas sensing property," *J. Rare Earths*, vol. 28, pp. 171–173, 2010.
- [21] Q. Xiang, G. Meng, Y. Zhang, J. Xu, P. Xu, Q. Pan, and W. Yu, "Ag nanoparticle embedded-ZnO nanorods synthesized via a photochemical method and its gas sensing properties," *Sens. Actuators B: Chem.*, vol. 143, pp. 635–640, 2010.
- [22] H. S. Woo, C. H. Kwak, J. H. Chung, and J. H. Lee, "Highly selective and sensitive xylene sensors using Ni-doped branched ZnO nanowire networks," *Sens. Actuators B: Chem.*, vol. 216, pp. 358–366, 2015.
- [23] S. Huang, T. Wang, and Q. Xiao, "Effect of Fe doping on the structural and gas sensing properties of ZnO porous microspheres," *J. Phys. Chem. Solids*, vol. 76, pp. 51–58, 2015.
- [24] D. Han, J. Yang, F. Gu, and Z. Wang, "Effects of rare earth elements doping on ethanol gas sensing performance of three-dimensionally ordered macroporous In₂O₃," *RSC Adv.*, 2013.
- [25] O. Singh and R. C. Singh, "Enhancement in ethanol sensing response by surface activation of ZnO with SnO₂," *Mater. Res. Bull.*, vol. 47, no. 3, pp. 557–561, 2012.
- [26] S. Bai, T. Guo, Y. Zhao, J. Sun, D. Li, A. Chen, and C. C. Liu, "Sensing performance and mechanism of Fe-doped ZnO microflowers," *Sens. Actuators B: Chem.*, vol. 195, pp. 657–666, 2014.
- [27] A. Mirzaei, J. H. Kim, H. W. Kim, and S. S. Kim, "Resistive-based gas sensors for detection of benzene, toluene, and xylene (BTX) gases: A review," *J. Mater. Chem. C*, vol. 6, pp. 4342–4370, 2018.
- [28] H. T. Derraz, N. Benramdane, D. Nacer, A. Bouzidi, and M. Medles, "Investigations on Zn_xCd_{1-x}O thin films obtained by spray pyrolysis," *Sol. Energy Mater. Sol. Cells*, vol. 73, pp. 249–259, 2002.
- [29] R. V. Kumar, K. J. Lethy, P. R. A. Kumar, R. R. Krishnan, N. V. Pillai, V. P. M. Pillai, and R. Philip, "Effect of cadmium oxide incorporation on the microstructural and optical properties of pulsed laser deposited nanostructured zinc oxide thin films," *Mater. Chem. Phys.*, vol. 121, pp. 406–413, 2010.
- [30] M. I. Khan, K. A. Bhatti, R. Quindeel, L. G. Bousiakou, N. Alonizan, and F. Alam, "Investigations of the structural, morphological, and electrical properties of multilayer ZnO/TiO₂ thin films deposited by sol-gel technique," *Results Phys.*, vol. 6, pp. 156–160, 2016.
- [31] J. K. Rajput, T. K. Pathak, V. Kumar, M. Kumar, and L. P. Purohit, "Annealing temperature dependent investigations on the nano-cauliflower-like structure of CdO thin film grown by sol-gel method," *Surf. Interfaces*, vol. 6, pp. 11–17, 2017.
- [32] W. Guo, T. Liu, R. Sun, Y. Chen, W. Zeng, and Z. Wang, "Hollow, porous, and yttrium functionalized ZnO nanospheres with enhanced gas-sensing performances," *Sens. Actuators B: Chem.*, vol. 178, pp. 53–62, 2013.
- [33] V. S. Rana, J. K. Rajput, T. K. Pathak, and L. P. Purohit, "Multilayer MgZnO/ZnO thin films for UV photodetectors," *J. Alloys Compd.*, vol. 764, pp. 724–729, 2018.
- [34] M. Thirumoorthi and J. H. J. Prakash, "Structural, morphological characteristics and optical properties of Y-doped ZnO thin films by sol-gel spin coating method," *Superlattices Microstruct.*, vol. 85, pp. 237–247, 2015.
- [35] V. S. Rana, J. K. Rajput, T. K. Pathak, and L. P. Purohit, "Cu sputtered Cu/ZnO Schottky diode on fluorine-doped tin oxide substrate for optoelectronic applications," *Thin Solid Films*, vol. 679, pp. 79–85, 2019.

- [36] S. Ilicon, M. Caglar, and Y. Caglar, "Sn doping effects on the electro-optical properties of sol-gel derived transparent ZnO films," *Appl. Surf. Sci.*, vol. 256, pp. 7204–7210, 2010.
- [37] M. Caglar, Y. Caglar, S. Aksoy, and S. Silicon, "Temperature dependence of the optical bandgap and electrical conductivity of sol-gel derived undoped and Li-doped ZnO films," *Appl. Surf. Sci.*, vol. 256, pp. 4966–4971, 2010.
- [38] G. K. Upadhyay, J. K. Rajput, T. K. Pathak, H. C. Swart, and L. P. Purohit, "Photoactive CdO: TiO₂ nanocomposites for dyes degradation under visible light," *Mater. Chem. Phys.*, vol. 253, pp. 123191, 2020.
- [39] Z. Liu, B. Liu, W. Xie, H. Li, R. Zhou, Q. Li, and T. Wang, "Enhanced selective acetone sensing characteristics based on Co-doped WO₃ hierarchical flower-like nanostructures assembled with nanoplates," *Sens. Actuators B: Chem.*, vol. 235, pp. 614–621, 2016.
- [40] D. R. Miller, S. A. Akbar, and P. A. Morris, "Nanoscale metal oxide-based heterojunctions for gas sensing: A review," *Sens. Actuators B: Chem.*, vol. 204, pp. 250–272, 2014.